

# Estimating the silica content and loss-on-ignition in the North American Soil Geochemical Landscapes datasets: a recursive inversion approach

Patrice de Caritat<sup>1,\*</sup>, Eric C. Grunsky<sup>2</sup>, David B. Smith<sup>3</sup>

<sup>1</sup>Geoscience Australia, GPO Box 378, Canberra, ACT 2601, Australia

<sup>2</sup>Department of Earth & Environmental Sciences, University of Waterloo, Waterloo, ONT N2L 3G1, Canada, ORCID: 0000-0003-4521-163X

<sup>3</sup>International Union of Geological Sciences Commission on Global Geochemical Baselines, Wheat Ridge, CO 80033, USA

\*Corresponding author, Email: [Patrice.deCaritat@ga.gov.au](mailto:Patrice.deCaritat@ga.gov.au), Twitter: @Patdecar, ORCID: 0000-0002-4185-9124

## 1 ABSTRACT

---

A novel method of estimating the silica (SiO<sub>2</sub>) and loss-on-ignition (LOI) concentrations for the North American Soil Geochemical Landscapes (NASGL) project datasets is proposed. Combining the precision of the geochemical determinations with the completeness of the mineralogical NASGL data, we suggest a ‘reverse normative’ or inversion approach to calculate first the minimum SiO<sub>2</sub>, water (H<sub>2</sub>O) and carbon dioxide (CO<sub>2</sub>) concentrations in weight percent (wt%) in these samples. These can be used in a first step to compute minimum and maximum estimates for SiO<sub>2</sub>. In a recursive step, a ‘consensus’ SiO<sub>2</sub> is then established as the average between the two aforementioned estimates, trimmed as necessary to yield a total composition (major oxides converted from reported Al, Ca, Fe, K, Mg, Mn, Na, P, S, and Ti elemental concentrations + ‘consensus’ SiO<sub>2</sub> + reported trace element concentrations converted to wt% + ‘normative’ H<sub>2</sub>O + ‘normative’ CO<sub>2</sub>) of no more than 100 wt%. Any remaining compositional gap between 100 wt% and this sum is considered ‘other’ LOI and likely includes H<sub>2</sub>O and CO<sub>2</sub> from the reported ‘amorphous’ phase (of unknown geochemical or mineralogical composition) as well as other volatile components present in soil. We validate the technique against a separate dataset from Australia where geochemical (including all major oxides) and mineralogical data exist on the same samples. The correlation between predicted and observed SiO<sub>2</sub> is linear, strong ( $R^2 = 0.91$ ) and homoscedastic. We also compare the estimated NASGL SiO<sub>2</sub> concentrations with another publicly available continental-scale survey over the conterminous USA, the ‘Shacklette and Boerngen’ dataset. This comparison shows the new data to be a reasonable representation of SiO<sub>2</sub> values measured on the ground over the same study area. We recommend the approach of combining geochemical and mineralogical information to estimate missing SiO<sub>2</sub> and LOI by the recursive inversion approach in datasets elsewhere, with the caveat to validate results.

*Keywords:* SiO<sub>2</sub>, LOI, geochemical survey, geochemistry, mineralogy, compositional data, normative analysis

This is a non-peer reviewed preprint submitted to EarthArXiv; a manuscript has been submitted to the journal ‘Geochemistry: Exploration, Environment, Analysis’

## 2 INTRODUCTION

---

Rock, sediment and soil chemical and mineralogical characterizations are fundamental to the discipline of geochemistry, particularly when it comes to applications in the fields of mineral exploration, environmental management, agronomy, horticulture and forestry, and landuse decision making. Most rocks, sediments and soils on Earth contain minerals that include silicon (Si) and oxygen (O) in their structure (e.g., silicates), and often also hydrogen (H; e.g., phyllosilicates) and, perhaps less-commonly, carbon (C; e.g., carbonates) (e.g., Finkl 1981, Deer et al. 1992, Schaetzl & Anderson 2007). Traditionally, total analyses for major elements have been reported as oxides (the term 'major' is used here to include components with generally greater than 0.1 percent abundance), typically obtained using X-Ray Fluorescence (XRF) as the analytical method, which determines total content (regardless of the host, speciation or oxidation state of each major element). The analysis of rock, sediment and soil samples by XRF is often complemented by the gravimetric determination of 'loss-on-ignition' (LOI) obtained by heating the sample to a set temperature (e.g., 900 °C) and measuring the mass loss compared to the starting sample at standardized temperature, pressure and humidity. LOI has several components, including adsorbed water (H<sub>2</sub>O; e.g., interlayer water in clay minerals), combined H<sub>2</sub>O (e.g., hydrated minerals and labile hydroxyl-compounds), carbon dioxide (CO<sub>2</sub>; e.g., from carbonates and organic matter), and volatile elements (e.g., Hg).

One advantage of reporting the major components of a rock, sediment or soil sample as oxides is that their sum, when complemented by LOI and trace elements (TEs), should add up to 100 weight percent (wt%) of the sample. Having a complete sample analysis, or at least as complete as practically feasible, is important to give confidence that the sample is well characterized, which implies that the composition is closed or full and not a subcomposition. This has implications in subsequent data analytics, including in the development and application of Compositional Data Analysis (CoDA) methods (e.g., Chayes 1960, Aitchison 1986, Scealy et al. 2015).

Another benefit of a complete sample analysis is the direct relationship between the geochemical and mineralogical compositions, via the knowledge (or modeling) of the minerals' stoichiometric compositions. Deriving the most plausible mineralogy from geochemistry is a non-unique inversion problem known as 'normative analysis' (e.g., Caritat et al. 1994, Aldis et al. 2023). This is a very useful way to ensure that chemistry and mineralogy of a sample are mutually compatible, especially for finer-grained samples where optical or even electronic microscopic techniques reach their resolution limit to helpfully identify minerals.

In recent decades, another family of analytical methods has gained in popularity, mainly due to its high precision and multi-elemental capability, namely the Inductively Coupled Plasma-Atomic Emission Spectroscopy (ICP-AES) and -Mass Spectrometry (ICP-MS) methods. The ICP-based methods typically require a digestion of the rock, sediment or soil sample to present it to the instrument as a liquid phase (laser ablation is an alternative input mode not discussed here). This digestion, which can range from near-total to weak, and from selective to nonselective, is crucial to document in detail as it controls how to interpret the geochemical results (e.g., Mann 2010). ICP data often consist of a list of 30 or more elements, generally reported in parts per million mass/mass (ppm m/m; equivalent to mg/kg and µg/g). These element concentrations for the major elements (Al, Ca, Fe, etc.) can readily be converted to oxide equivalents (yielding a 'pseudo-XRF' result).

Generally a full or complete analysis of a rock, sediment or soil, expressed as oxides, consists of Al<sub>2</sub>O<sub>3</sub>, CaO, FeO, Fe<sub>2</sub>O<sub>3</sub>, K<sub>2</sub>O, MgO, MnO, Na<sub>2</sub>O, P<sub>2</sub>O<sub>5</sub>, SiO<sub>2</sub>, SO<sub>3</sub>, and TiO<sub>2</sub> concentrations typically

expressed in wt%, either directly obtained by XRF or converted from ICP elemental data. Often, the two Fe analytes, reduced and oxidized Fe, are reported together as Fe<sub>2</sub>O<sub>3tot</sub>. Added together and supplemented by LOI and TE concentrations, the full analysis is considered complete and should sum to (or close to) 100 wt%. Any discrepancy represents components not analyzed for and/or uncertainty.

### 3 THE NORTH AMERICAN SOIL GEOCHEMICAL LANDSCAPES PROJECT

---

The North American Soil Geochemical Landscapes (NASGL) project is a recent continental-scale geochemical survey of the conterminous United States of America (Smith et al. 2013, 2014, 2019; see recent project review in Smith 2022). It sampled soil from three levels (0-5 cm depth, A horizon and C horizon) at 4857 sites, the <2-mm fraction of which was analyzed for 45 major and trace element concentrations by methods yielding ‘total or near-total’ elemental content. The chemical elements reported were Ag, Al, As, Ba, Be, Bi, C, Ca, Cd, Ce, Co, Cr, Cs, Cu, Fe, Ga, Hg, In, K, La, Li, Mg, Mn, Mo, Na, Nb, Ni, P, Pb, Rb, S, Sb, Sc, Se, Sn, Sr, Te, Th, Ti, Tl, U, V, W, Y, and Zn. Elements were mostly analyzed and quantified by ICP-AES or ICP-MS, after a four-acid (hydrochloric, nitric, hydrofluoric, and perchloric acids) digestion of the milled samples at a temperature of between 125 and 150 °C (see Smith et al. 2013 for more detail). Note that Si was not included in the contracted analytical package. As ICP-based analytical techniques cannot quantify O and H present (in fact, abundant) in most if not all rock, sediment, or soil sample, the sum of all its analytes (Al, ..., Zn) falls well short of one million ppm (a complete composition); indeed in the C horizon dataset, for instance, the sum of all ICP analytes ranges from 1134 to 390,740 ppm (average 144,869 ppm). Table 1 presents a brief statistical summary of the geochemical composition of NASGL C horizon soils for the major elements. The C horizon dataset is used herein to illustrate our method.

*Table 1. Summary statistics (count, minimum, median, average, maximum and standard deviation, in ppm) for the major elements aluminum (Al), calcium (Ca), iron (Fe), potassium (K), magnesium (Mg), manganese (Mn), sodium (Na), phosphorus (P), sulfur (S), and titanium (Ti) in the C horizon samples from the NASGL project (source: Smith et al. 2013).*

Element	Count	Min	Med	Ave	Max	SD
<b>Al</b>	4669	200	53900	54441	186000	23214
<b>Ca</b>	4669	2.26	10600	26452	323000	40091
<b>Fe</b>	4669	89.5	23400	26292	153000	16765
<b>K</b>	4669	16.3	15300	15073	56700	7607
<b>Mg</b>	4669	8.76	6100	8189	168000	8460
<b>Mn</b>	4669	2.47	390	503	12000	567
<b>Na</b>	4669	2.28	6900	8184	55400	6975
<b>P</b>	4669	11.5	420	508	27400	632
<b>S</b>	4669	1.31	200	1087	162000	7626
<b>Ti</b>	4669	72.7	2600	2916	34200	1980
<b>Sum Majors</b>	4669	1106	143683	143645	389889	61524
<b>Sum All ICP</b>	4669	1134	145149	144869	390740	61897

The NASGL project also analyzed and quantified mineralogy in those samples. The minerals quantified were quartz, K-feldspars, plagioclases, (total feldspars), 14 Å clays, 10 Å clays, kaolinite, (total clays), gibbsite, calcite, dolomite, aragonite, (total carbonates), analcime, heulandite, (total

zeolites), gypsum, talc, hornblende, serpentine, hematite, goethite, pyroxene, pyrite, other, and amorphous (phases in parenthesis are summations of other minerals). The amorphous phase typically consists of material that is poorly diffracting; this will generally include clay minerals, various forms of micro-quartz, Fe-, Mn- and Al-oxyhydroxides, organic matter, volcanic glass, etc. (e.g., Tan et al. 1970, Smith et al. 2018, Tsukimura et al. 2021). Minerals were analyzed by X-Ray Diffraction (XRD) and quantified using a Rietveld refinement method (Smith et al. 2013). Unlike the geochemical data, the XRD data are ‘complete’ in the sense that they add up to 100 wt% (range 99.6 to 100.2 wt%, average 100.03 wt%, for the C horizon). Table 2 presents a brief statistical summary of the mineralogical composition of NASGL C horizon soils.

*Table 2. Summary statistics (count, minimum, median, average, maximum and standard deviation, in wt%) for the minerals quartz (Quartz), K-feldspars (Tot\_K\_fs), plagioclases (Tot\_Plug), total feldspars (Tot\_Flds), 14 Å clays (Tot\_14A), 10 Å clays (Tot\_10A), kaolinite (Kaolinit), total clays (Tot\_Clay), gibbsite (Gibbsite), calcite (Calcite), dolomite (Dolomite), aragonite (Aragon), total carbonates (Tot\_Carb), analcime (Analcime), heulandite (Heuland), total zeolites (Tot\_Zeol), gypsum (Gypsum), talc (Talc), hornblende (Hornbl), serpentine (Serpent), hematite (Hematite), goethite (Goethite), pyroxene (Pyroxene), pyrite (Pyrite), other (Other), and amorphous (Amorph) in the C horizon samples from the NASGL project (source: Smith et al. 2013).*

<b>Mineral</b>	<b>Count</b>	<b>Min</b>	<b>Med</b>	<b>Ave</b>	<b>Max</b>	<b>SD</b>
<b>Quartz</b>	4660	0	44	46.1	99.4	23.0
<b>Tot_K_fs</b>	3966	0	3.7	4.9	45.2	5.3
<b>Tot_Plug</b>	3844	0	7.7	11.0	67.0	11.5
<b>Tot_Flds</b>	4280	0	12.6	16.0	80.1	14.5
<b>Tot_14A</b>	2461	0	0.6	2.6	44.1	3.9
<b>Tot_10A</b>	4248	0	7.2	8.1	65.1	6.0
<b>Kaolinit</b>	1989	0	0	2.8	79.9	6.8
<b>Tot_Clay</b>	4513	0	11.7	13.6	86.3	10.0
<b>Gibbsite</b>	122	0	0	0.2	30.4	1.3
<b>Calcite</b>	1801	0	0	3.5	84.1	8.5
<b>Dolomite</b>	846	0	0	1.4	81.4	4.6
<b>Aragon</b>	38	0	0	0.1	65.3	1.2
<b>Tot_Carb</b>	1939	0	0	5.0	84.1	10.3
<b>Analcime</b>	15	0	0	0.01	9.2	0.3
<b>Heuland</b>	56	0	0	0.1	38.0	0.9
<b>Tot_Zeol</b>	71	0	0	0.1	38.0	0.9
<b>Gypsum</b>	208	0	0	0.4	96.5	4.2
<b>Talc</b>	26	0	0	0.02	16.4	0.4
<b>Hornbl</b>	821	0	0	0.4	62.6	1.8
<b>Serpent</b>	9	0	0	0.01	26.7	0.4
<b>Hematite</b>	313	0	0	0.1	13.5	0.5
<b>Goethite</b>	184	0	0	0.1	14.1	0.6
<b>Pyroxene</b>	147	0	0	0.3	33.6	2.1
<b>Pyrite</b>	3	0	0	0.0002	0.4	0.01
<b>Other</b>	66	0	0	0.1	35.9	1.4
<b>Amorph</b>	4327	0	17.5	17.8	95.2	12.0

One of the shortcomings of the NASGL project is that neither Si/SiO<sub>2</sub> nor LOI were reported in the released geochemical datasets. The present contributions aims to propose and test a method for estimating those missing, yet crucial, parameters.

## 4 ESTIMATING SiO<sub>2</sub> AND LOI FROM GEOCHEMISTRY AND MINERALOGY

As the NASGL project did not use XRF analysis, we first need to convert the 10 reported major elements (Al, Ca, Fe, K, Mg, Mn, Na, P, S, and Ti) into oxides, which is readily achieved by dividing each elemental concentration by the atomic weight of the element, multiplying this by the molecular weight of the oxide, and adjusting for any unit change (e.g., dividing by 10,000 to convert from ppm to wt%). These oxides are hereafter referred to as other\_oxides to indicate that they do not include SiO<sub>2</sub>. For one of the most common soil components, Si, no reported elemental or oxide concentration exists and it must thus be estimated. The proposed method for estimating SiO<sub>2</sub>, which draws upon both the geochemical and the mineralogical analyses of the NASGL samples, is described below and the workflow illustrated in Figure 1. A worked example is provided as a Microsoft Excel spreadsheet (see Section 6).

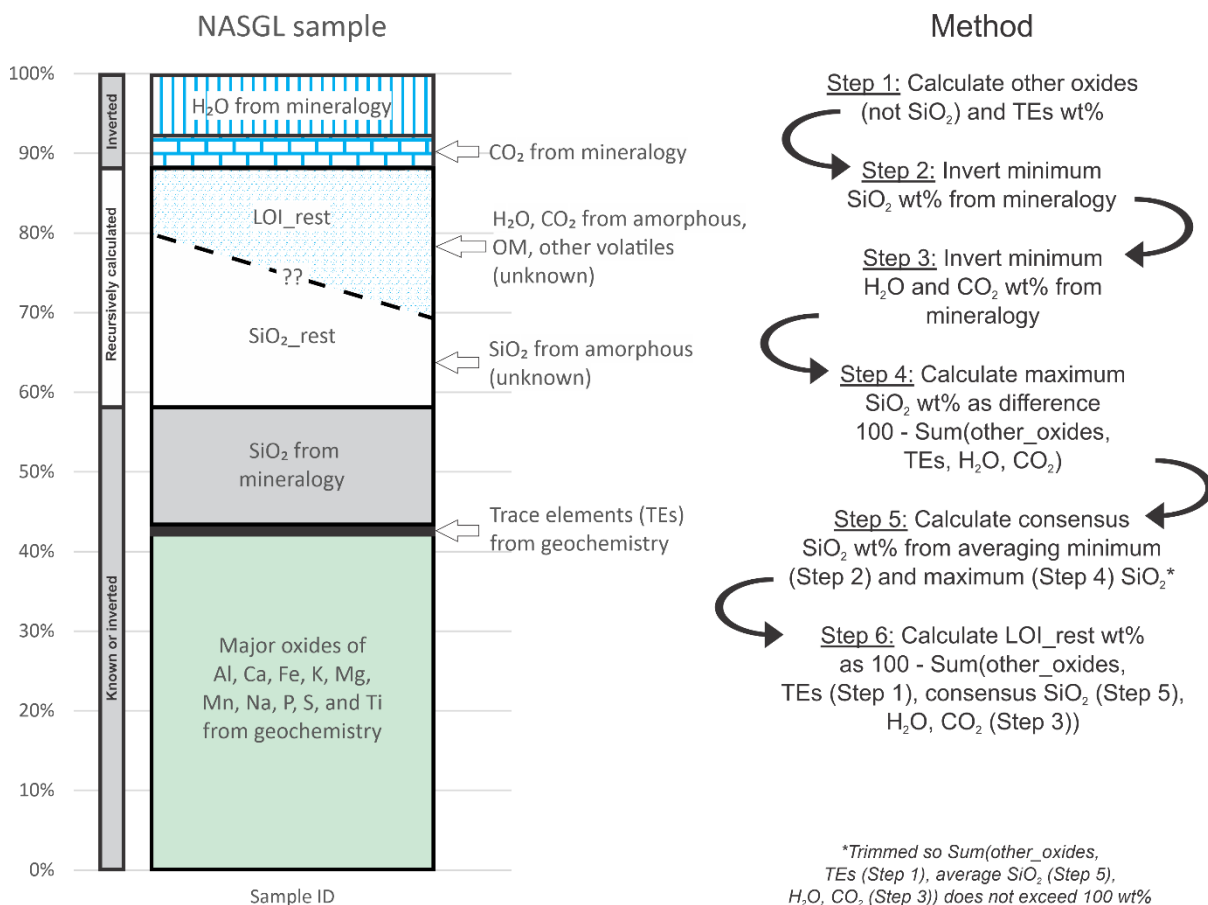


Figure 1. Conceptual diagram of an incomplete rock, sediment, or soil analysis and workflow of the SiO<sub>2</sub> and LOI recursive inversion estimation methodology developed herein using geochemistry and mineralogy.

Initially, two estimates for SiO<sub>2</sub> are calculated by inverting mineralogical information; neither is ideal, as the first is likely to give a minimum, the second a maximum value for SiO<sub>2</sub>. Next, a 'consensus'

SiO<sub>2</sub> concentration is obtained recursively from the two aforementioned estimates. Finally, the LOI is calculated to obtain a closed full composition at 100 wt%. The detailed steps are described below.

**Step 1: Data preparation.** The geochemical and mineralogical data for soils of the conterminous United States (A and C horizon datasets) were downloaded from <https://mrdata.usgs.gov/ds-801/>. Samples (rows) which had either incomplete or missing geochemical or mineralogical quantification (e.g., insufficient sample material) were removed. Analytes (columns) with excessive censored values (below detection/reportable limit) were removed (e.g., Ag, Cs, Te; Grunsky et al. 2018). Concentration units were unified (ppm) and censored data were imputed using the zCompositions package (IrEM function) in the R computing environment (Palarea-Albaladejo et al. 2014). Note that the imputation step is not critical to the present estimation workflow and other ways of handling censored data may be applied. After imputation, the major elements were converted to oxides and all analytes were expressed as wt%.

**Step 2: Inverting ‘normative’ SiO<sub>2</sub> due to silicate minerals.** The ‘normative’ SiO<sub>2</sub> is the amount of SiO<sub>2</sub> each sample must contain to be consistent with its mineralogy (technically this is a reverse normative or inversion approach). This ‘normative’ SiO<sub>2</sub> calculates and sums the contributions in SiO<sub>2</sub> of each Si-bearing mineral (silicate), for example, **1 \* quartz + 0.6476 \* K-feldspar + ... + AVERAGE (0.483, 0.5985, 0.5549, 0.5173) \* pyroxene**. The multipliers are the mass proportions of the relevant oxide (e.g., SiO<sub>2</sub>) in each mineral (e.g., K-feldspar above), and were sourced from <https://webmineral.com>. Where more than one end-member mineral exists for a group (e.g., a solid-solution), the average of the (most common) end-members is used (e.g., pyroxene above). Table 3 summarizes the proportional multipliers used in this paper. This first estimate of SiO<sub>2</sub> does not consider the phases ‘other’ and ‘amorphous’. Amorphous has a median abundance of 17.5 wt% and a maximum of 95.2 wt% in the NASGL C horizon dataset. It is likely to contain forms of microcrystalline silica, such as opal-A; e.g., Achilles et al. 2018), and therefore the ‘normative’ SiO<sub>2</sub> calculated here could, and most likely does, underestimate the real SiO<sub>2</sub> concentration.

*Table 3. Mineral formulas and silica (SiO<sub>2</sub>), water (H<sub>2</sub>O) and carbon dioxide (CO<sub>2</sub>) proportions (in wt%) for the minerals in the C horizon samples from the NASGL project (source: <https://webmineral.com>). Pyroxene minerals are grouped as clinopyroxene (cpx) or orthopyroxene (opx).*

Mineral	Group	Formula	SiO <sub>2</sub>	H <sub>2</sub> O	CO <sub>2</sub>
Quartz		SiO <sub>2</sub>	100	0	0
Orthoclase	Feldspar	KAlSi <sub>3</sub> O <sub>8</sub>	64.76	0	0
Albite	Plagioclase	Na <sub>0.95</sub> Ca <sub>0.05</sub> Al <sub>1.05</sub> Si <sub>2.95</sub> O <sub>8</sub>	67.39	0	0
Anorthite	Plagioclase	Na <sub>0.05</sub> Ca <sub>0.95</sub> Al <sub>1.95</sub> Si <sub>2.05</sub> O <sub>8</sub>	44.40	0	0
Clinocllore	Chlorite (14 Å)	Mg <sub>3.75</sub> Fe <sup>2+</sup> <sub>1.25</sub> Si <sub>3</sub> Al <sub>2</sub> O <sub>10</sub> (OH) <sub>8</sub>	30.28	12.11	0
Chamosite	Chlorite (14 Å)	Fe <sup>2+</sup> <sub>3</sub> Mg <sub>1.5</sub> AlFe <sup>3+</sup> <sub>0.5</sub> Si <sub>3</sub> AlO <sub>12</sub> (OH) <sub>6</sub>	27.14	8.14	0
Illite	Illite (10 Å)	K <sub>0.6</sub> (H <sub>3</sub> O) <sub>0.4</sub> Al <sub>1.3</sub> Mg <sub>0.3</sub> Fe <sup>2+</sup> <sub>0.1</sub> Si <sub>3.5</sub> O <sub>10</sub> (OH) <sub>2</sub> · (H <sub>2</sub> O)	54.01	12.03	0
Kaolinite		Al <sub>2</sub> Si <sub>2</sub> O <sub>5</sub> (OH) <sub>4</sub>	46.55	13.96	0
Gibbsite		Al(OH) <sub>3</sub>	0	34.64	0

Mineral	Group	Formula	SiO <sub>2</sub>	H <sub>2</sub> O	CO <sub>2</sub>
Calcite	Carbonate	CaCO <sub>3</sub> (trigonal)	0	0	43.97
Dolomite	Carbonate	CaMg(CO <sub>3</sub> ) <sub>2</sub>	0	0	47.73
Aragonite	Carbonate	CaCO <sub>3</sub> (orthorhombic)	0	0	43.97
Analcime	Zeolite	NaAl(Si <sub>2</sub> O <sub>6</sub> )•(H <sub>2</sub> O)	54.58	8.18	0
Heulandite-Ca	Zeolite	Ca <sub>3.57</sub> Sr <sub>0.05</sub> Ba <sub>0.06</sub> Mg <sub>0.01</sub> Na <sub>1.26</sub> K <sub>0.43</sub> Al <sub>9.37</sub> Si <sub>26.7</sub> O <sub>72</sub> •26.02(H <sub>2</sub> O)	56.78	16.59	0
Heulandite-K	Zeolite	K <sub>2.4</sub> Na <sub>0.96</sub> Ca <sub>1.64</sub> Mg <sub>0.64</sub> Sr <sub>0.56</sub> Ba <sub>0.12</sub> Al <sub>9.08</sub> Fe <sup>3+</sup> <sub>0.56</sub> Si <sub>26.48</sub> O <sub>72</sub> •25.84(H <sub>2</sub> O)	54.86	16.05	0
Gypsum		Ca(SO <sub>4</sub> )•2(H <sub>2</sub> O)	0	20.93	0
Talc		Mg <sub>3</sub> Si <sub>4</sub> O <sub>10</sub> (OH) <sub>2</sub>	63.37	4.75	0
Magnesian-hornblende	Hornblende	Ca <sub>2</sub> Mg <sub>4</sub> Al <sub>0.75</sub> Fe <sup>3+</sup> <sub>0.25</sub> (Si <sub>7</sub> AlO <sub>22</sub> )(OH) <sub>2</sub>	51.22	2.19	0
Clinochrysotile	Serpentine	Mg <sub>3</sub> Si <sub>2</sub> O <sub>5</sub> (OH) <sub>4</sub>	43.36	13.00	0
Hematite		Fe <sup>3+</sup> <sub>2</sub> O <sub>3</sub>	0	0	0
Goethite		Fe <sup>3+</sup> O(OH)	0	10.14	0
Augite	Pyroxene (cpx)	Ca <sub>0.9</sub> Na <sub>0.1</sub> Mg <sub>0.9</sub> Fe <sup>2+</sup> <sub>0.2</sub> Al <sub>0.4</sub> Ti <sub>0.1</sub> Si <sub>1.9</sub> O <sub>6</sub>	48.30	0	0
Diopside	Pyroxene (cpx)	CaMg(Si <sub>2</sub> O <sub>6</sub> )	55.49	0	0
Enstatite	Pyroxene (opx)	Mg <sub>2</sub> Si <sub>2</sub> O <sub>6</sub>	59.85	0	0
Ferrosilite	Pyroxene (opx)	Fe <sup>2+</sup> MgSi <sub>2</sub> O <sub>6</sub>	51.73	0	0
Pyrite		Fe <sup>2+</sup> S <sub>2</sub>	0	0	0

Step 3: Inverting LOI due to hydrate and carbonate minerals. The ‘**normative**’ H<sub>2</sub>O and ‘**normative**’ CO<sub>2</sub> components of LOI in each sample were calculated to be consistent with the mineralogy (e.g., amounts of gypsum and calcite). This is done in a similar way as described above, but applied to all O- and H-bearing (hydrate) minerals and all C-bearing (carbonate) minerals, respectively. The relevant proportional multipliers used are also given in Table 3. As for SiO<sub>2</sub>, the ‘**normative**’ H<sub>2</sub>O and CO<sub>2</sub> contents of the amorphous phase are not known and likely important (e.g., Achilles et al. 2018). Thus this method could, and most likely does, underestimate the real LOI concentration.

Step 4: Calculating a second estimate for SiO<sub>2</sub>. A second (maximum) SiO<sub>2</sub> estimate is calculated by the difference **100 wt% - Sum(other\_oxides, TEs, ‘normative’ H<sub>2</sub>O, ‘normative’ CO<sub>2</sub>)**. It could, and most likely does, overestimate the real SiO<sub>2</sub> concentration because LOI is almost certainly underestimated (see above). Note that in some instances, the first estimate of SiO<sub>2</sub> is larger than the second, which we interpret to result either from uncertainty in the mineralogical quantification (amounts of silicate, hydrate and carbonate minerals are not consistent with the geochemistry), or from overestimation of ‘**normative**’ H<sub>2</sub>O (‘**normative**’ CO<sub>2</sub> being well constrained by carbonate minerals).

Step 5: Recursively estimating a ‘consensus’ SiO<sub>2</sub>. A ‘consensus’ SiO<sub>2</sub> is then calculated recursively by first taking the average of the above two SiO<sub>2</sub> estimates. For some samples, this SiO<sub>2</sub> estimate results in the **Sum(all\_oxides, TEs, ‘normative’ H<sub>2</sub>O, ‘normative’ CO<sub>2</sub>)**, where all\_oxides include the ‘consensus’ SiO<sub>2</sub> determined at Step 4, to exceed 100 wt%; in these cases, the SiO<sub>2</sub> estimate is trimmed so that this sum is 100 wt%.

Step 6: Calculating total LOI. Finally, the **LOI\_rest**, that is volatiles others than the ‘normative’ H<sub>2</sub>O and ‘normative’ CO<sub>2</sub> calculated at Step 3 above, are calculated as the difference **100 wt% - Sum(all\_oxides, TEs, ‘normative’ H<sub>2</sub>O, ‘normative’ CO<sub>2</sub>)**. This LOI\_rest is likely to comprise H<sub>2</sub>O and CO<sub>2</sub> in the amorphous phase as well as any other volatiles not specifically accounted for above. From here, total LOI or LOI<sub>tot</sub> is calculated as **Sum(‘normative’ H<sub>2</sub>O, ‘normative’ CO<sub>2</sub>, LOI\_rest)**. Note that in a few cases where LOI<sub>tot</sub> is zero it is replaced by 0.0001 wt% to allow log-transformation.

## 5 RESULTS AND DISCUSSION

---

### 5.1 DISTRIBUTIONS OF THE SiO<sub>2</sub> AND LOI ESTIMATES

The resultant final estimates for SiO<sub>2</sub> in the C horizon samples from the NASGL project have a distribution as represented in the Tukey boxplots (Tukey 1977) of Figure 2, which seem reasonable compared to the distribution of the other oxides. SiO<sub>2</sub> is clearly the most abundant major oxide in the NASGL soils, as is both expected and consistent with other regions (e.g., Australia, see Caritat & Cooper 2011a). The distribution of LOI is also illustrated in Figure 2. Table 4 summarizes the statistics of the estimated SiO<sub>2</sub> and LOI concentrations derived herein for both the A and C horizons.

*Table 4. Summary statistics (count, minimum, median, average, maximum and standard deviation, in ppm) for the SiO<sub>2</sub> and LOI estimates in the A and C horizon samples from the NASGL project.*

Variable	Count	Min	Med	Ave	Max	SD
SiO <sub>2</sub> -A horizon	4800	7.25	72.02	72.07	99.80	13.96
SiO <sub>2</sub> -C horizon	4669	6.78	67.37	67.44	99.63	15.18
LOI-A horizon	4800	0.0001	8.20	8.99	44.87	6.57
LOI-C horizon	4669	0.0001	8.36	9.48	47.57	7.02

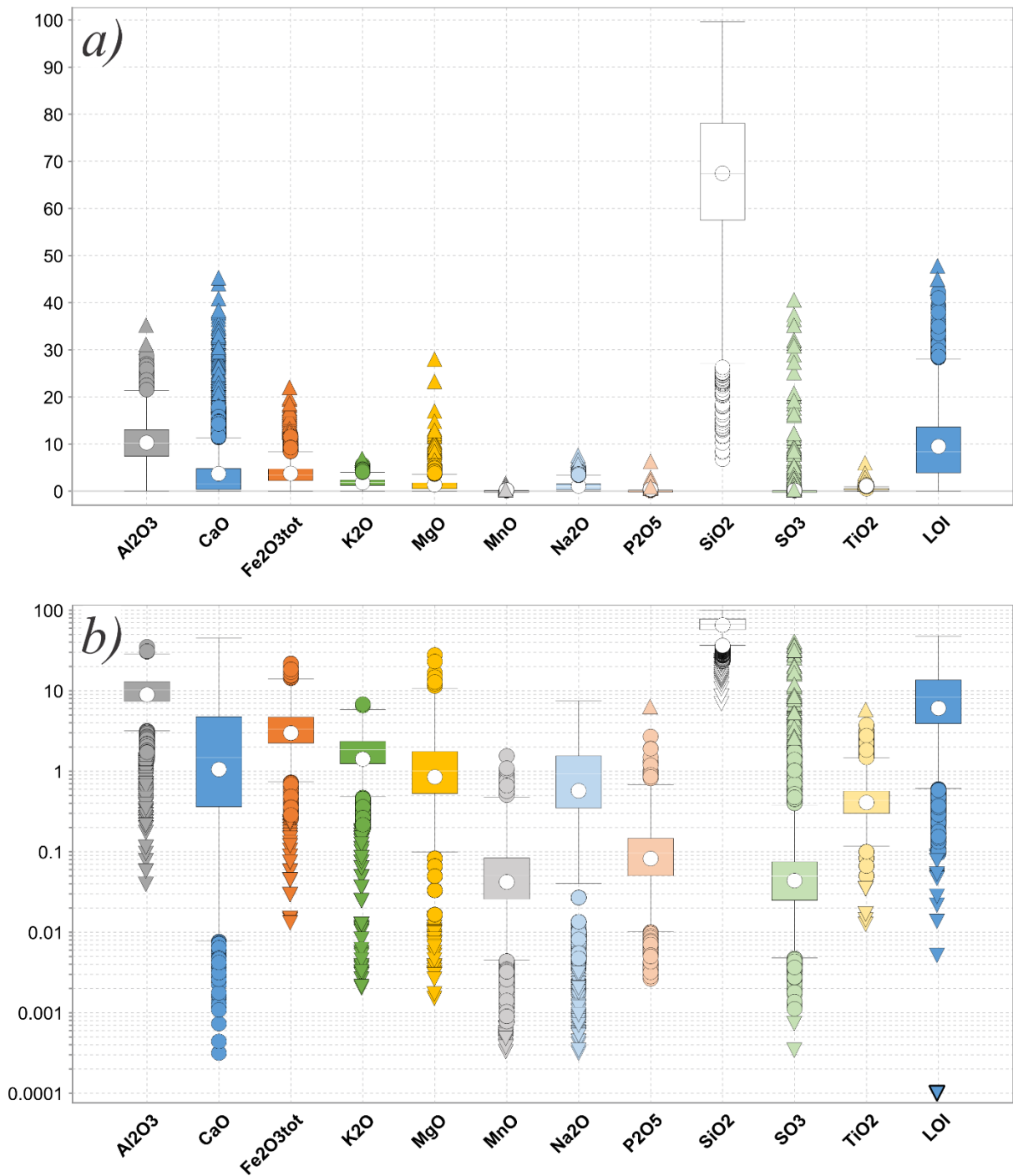


Figure 2. Tukey boxplots for the major oxides (wt%) in the C horizon samples from the NASGL project (source: Smith et al. 2013), including SiO<sub>2</sub> and LOI estimated by the method described herein, with a linear (a) and log ordinate scale (b). Each box spans the 25<sup>th</sup> to 75<sup>th</sup> percentile (a.k.a. the interquartile range, IQR), the median is represented by a white/grey line inside the box, the mean by a white dot, the whiskers by T-shaped bars extending 1.5 x IQR away from the box, the inner outliers (up to 3 x IQR away from the box) by circles, and the outer outliers (more than 3 x IQR away from the box) by triangles.

Figure 3 shows the cumulative frequency distributions of all major oxides, include SiO<sub>2</sub> and LOI<sub>tot</sub> estimated here. Note that in Figure 3, the concentration data have been Box-Cox transformed (Box & Cox 1964) to improve normality and homoscedasticity according to:

$$y_i^{(\lambda)} = \begin{cases} \frac{y_i^\lambda - 1}{\lambda} & \text{if } \lambda \neq 0, \\ \ln y_i & \text{if } \lambda = 0, \end{cases}$$

where the exponent  $\lambda$  is optimized for each variable  $y_i$  and reported in Table 5.

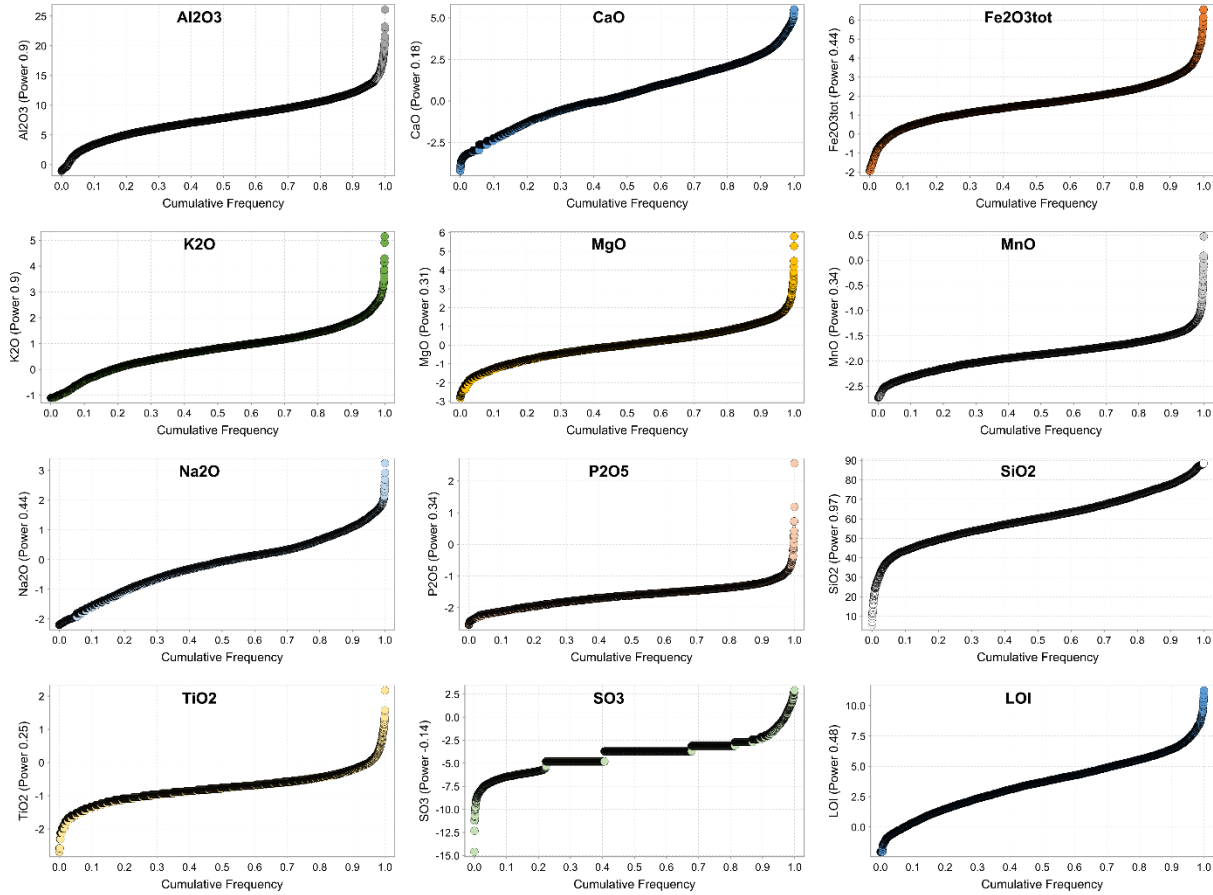


Figure 3. Cumulative frequency plots of the Box-Cox transformed major oxides (wt%) in the C horizon samples from the NASGL project (source: Smith et al. 2013), including  $\text{SiO}_2$  and LOI estimated by the method described herein. Note the Box-Cox transform power coefficient  $\lambda$  is indicated on the ordinate of each plot (see text).

Table 5. Box-Cox  $\lambda$  coefficients applied to the various major oxides in the C horizon samples from the NASGL project, including  $\text{SiO}_2$  and LOI estimated by the method described herein.

Element	$\lambda$	Element	$\lambda$	Element	$\lambda$
$\text{Al}_2\text{O}_3$	0.90	$\text{MgO}$	0.31	$\text{SiO}_2$	0.97
$\text{CaO}$	0.18	$\text{MnO}$	0.34	$\text{TiO}_2$	0.25
$\text{Fe}_2\text{O}_{3\text{tot}}$	0.44	$\text{Na}_2\text{O}$	0.44	$\text{SO}_3$	-0.14
$\text{K}_2\text{O}$	0.90	$\text{P}_2\text{O}_5$	0.34	<b>LOI</b>	0.48

## 5.2 APPLICATION TO SELECTED NASGL SAMPLES

Figure 4 shows the major oxide, including the  $\text{SiO}_2$  estimated as described above, TEs, 'normative'  $\text{H}_2\text{O}$ , 'normative'  $\text{CO}_2$ , and LOI\_rest of five selected samples from the NASGL C horizon dataset. Those samples were deliberately chosen to span the range of soil compositions in the dataset: sample from SiteID 7327 (California) is an Al-rich sample, 972 (Texas) is Ca-rich, 444 (Maryland) is Fe-rich, 12779 (Colorado) is K-rich, and 3808 (Florida) is Si-rich. Without the estimates for  $\text{SiO}_2$  and LOI (and its components), only between 0.2 (3808) and 54 wt% (972) of those samples would be geochemically characterized; the rest would be unknown. This unknown 'gap' is shown by the present estimation technique to comprise widely varying proportions of  $\text{SiO}_2$  (from silicates),  $\text{H}_2\text{O}$  (mainly from silicates),  $\text{CO}_2$  (from carbonates), and other volatile phases (from the amorphous phase and possibly other volatile components). It is thus important to provide estimates for each sample that honor the known mineralogical characteristics rather than apply a one-size-fits-all estimation of these parameters. Table 6 shows the mineralogy and geochemistry, including the 'gap'-filling  $\text{SiO}_2$  and LOI estimates, for these five samples.

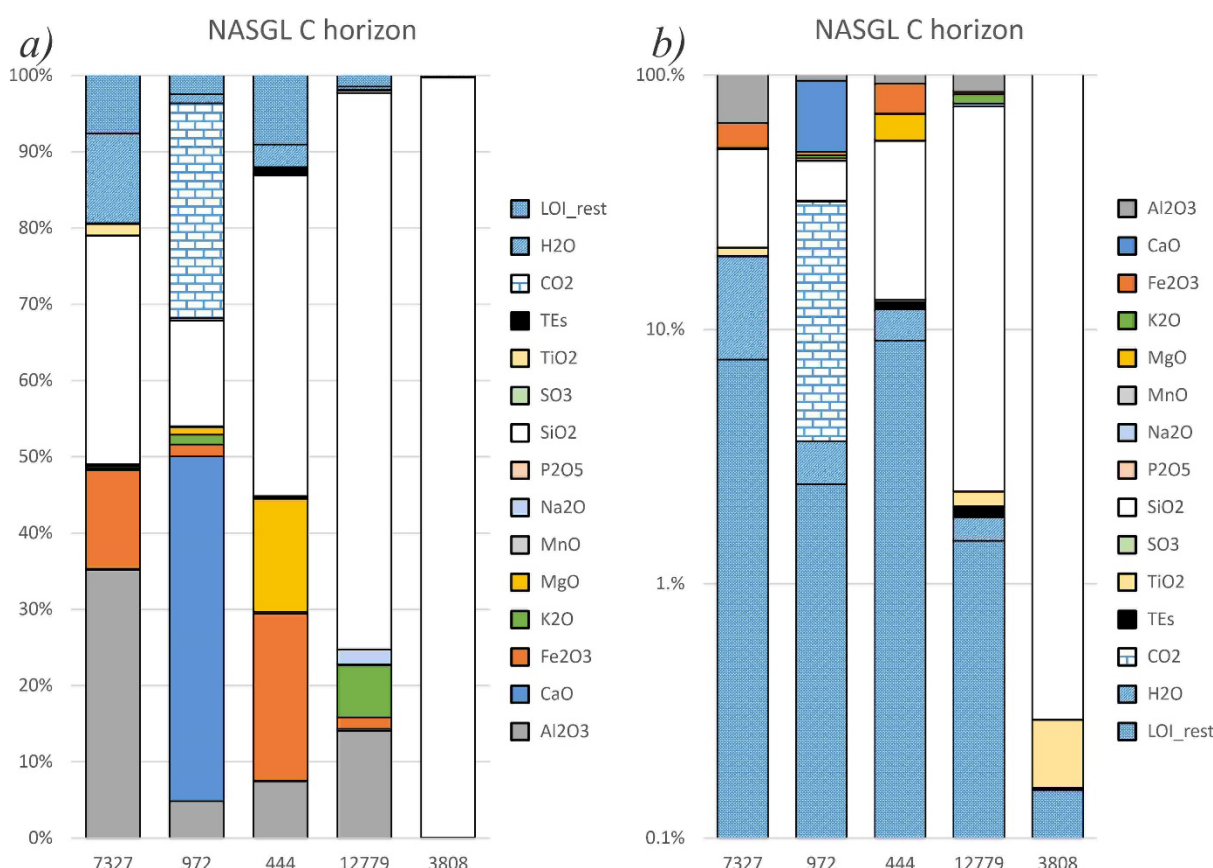


Figure 4. Bar graphs showing the composition of five selected C horizon samples from the NASGL project (source: Smith et al. 2013) in terms of major oxides (wt%), including  $\text{SiO}_2$  (white) and LOI (white with blue patterns) estimated by the method described herein, and trace elements (TEs). Components shown in conventional order with a linear scale (a) and on a log scale in reverse order to emphasize the LOI, TEs, and  $\text{TiO}_2$  components (b).

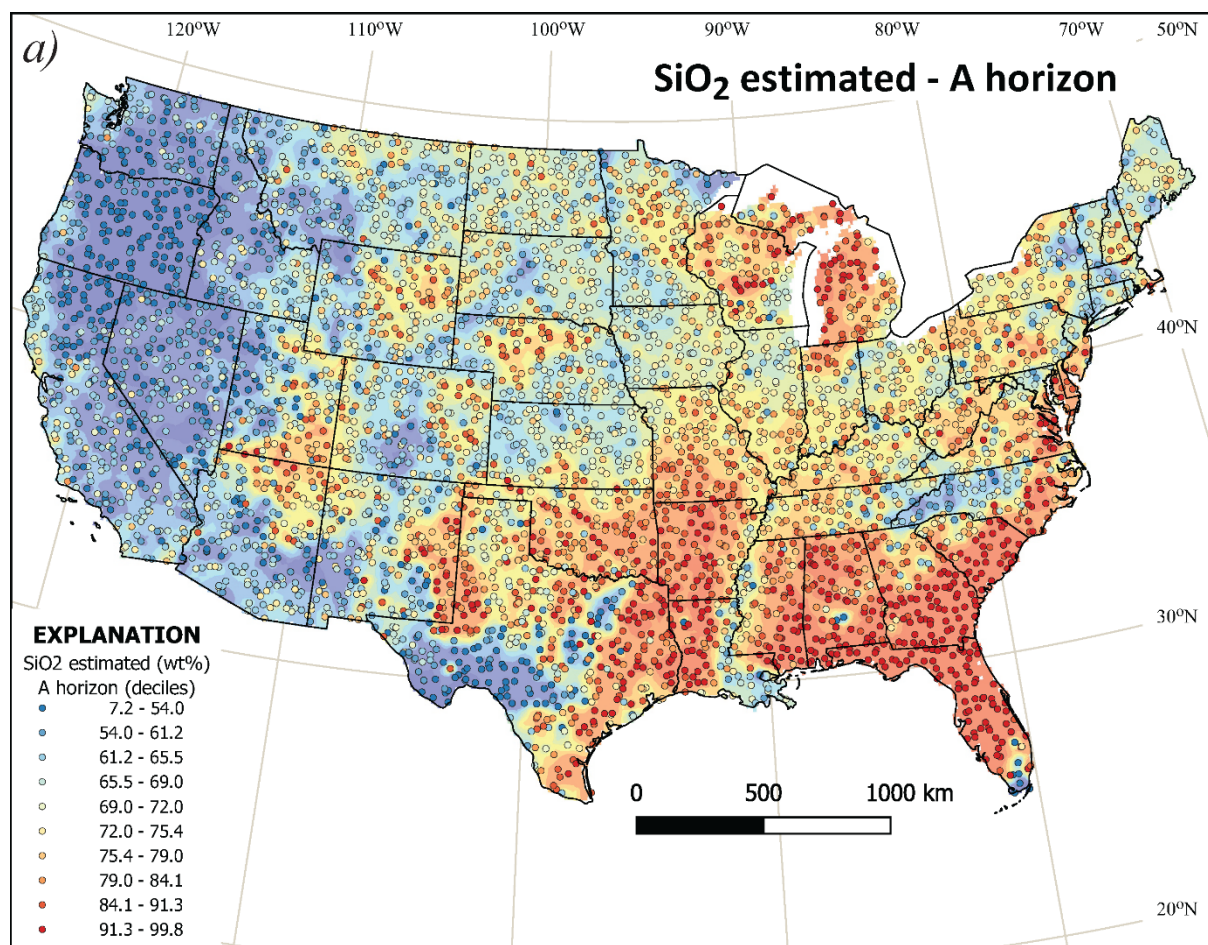
Table 6. Quantitative mineralogy and major oxide geochemistry (both in wt%) of the five selected C horizon samples from the NASGL project, including SiO<sub>2</sub> and LOI estimated by the method described herein.

SiteID	7327	972	444	12779	3808
<b>Site Information</b>					
StateID	CA	TX	MD	CO	FL
Latitude	39.1290	30.0131	39.3912	38.9289	28.1224
Longitude	-120.8070	-98.8698	-76.8290	-104.5352	-81.0767
LandCover1	Forested Upland	Herbaceous Upland	Forested Upland	Herbaceous Upland	Planted/Cultivated
LandCover2	Mixed Forest	Grasslands/Herbaceous	Deciduous Forest	Grasslands/Herbaceous	Urban/Recreational Grasses
Depth	80-96	30-50	70-78	70-85	70-100
Layer	C	C	C	C	C
<b>Mineralogy (wt%)</b>					
Quartz	3.1	6.3	16.3	32.3	98.5
Tot_K_fs	0	0	0	45.2	1.5
Tot_Plag	0.7	0	0	14.9	0
Tot_Flds	0.7	0	0	60	1.5
Tot_14Å	0	0	16.1	0	0
Tot_10Å	0	9.4	0	2.9	0
Kaolinit	40.5	0	8	0	0
Tot_Clay	40.5	9.4	24.2	2.9	0
Gibbsite	17.6	0	0	0	0
Calcite	0	64.1	0	0	0
Dolomite	0	0	0	0	0
Aragon	0	0	0	0	0
Tot_Carb	0	64.1	0	0	0
Analcime	0	0	0	0	0
Heuland	0	0	0	0	0
Tot_Zeol	0	0	0	0	0
Gypsum	0	0	0	0	0
Talc	0	0	4.1	0	0
Hornbl	0	0	0	0	0
Serpent	0	0	0	0	0
Hematite	4.5	0	3.8	0	0
Goethite	0	0.4	0	0	0
Pyroxene	0	0	10.7	0	0
Pyrite	0	0	0	0	0
Other	0	0	0	0	0
Amorph	33.7	19.8	41	4.8	0
<b>Geochemistry (wt%)</b>					
Al <sub>2</sub> O <sub>3</sub>	35.14	4.84	7.44	14.04	0.06
CaO	0.18	45.20	0.08	0.28	0.001
Fe <sub>2</sub> O <sub>3</sub> tot	12.91	1.59	21.87	1.50	0.01
K <sub>2</sub> O	0.23	1.28	0.29	6.83	0.003
MgO	0.27	0.99	14.77	0.13	0.002
MnO	0.05	0.05	0.19	0.02	0.000
Na <sub>2</sub> O	0.08	0.03	0.07	1.93	0.001
P <sub>2</sub> O <sub>5</sub>	0.17	0.03	0.12	0.02	0.01
SO <sub>3</sub>	0.05	0.07	0.05	0.01	0.001
TiO <sub>2</sub>	1.47	0.22	0.20	0.28	0.13
SiO <sub>2</sub> _est	29.95	13.84	42.07	72.94	99.63
LOI_est	19.36	31.82	12.00	1.82	0.15

For instance, sample 7327 contains significant clays (40.5 wt% kaolinite) and thus has not only elevated  $\text{Al}_2\text{O}_3$ , but also  $\text{SiO}_2$  and LOI ( $\text{H}_2\text{O}$ ) concentrations. Sample 972 holds significant carbonates (64.1 wt% calcite) as reflected not only by the elevated  $\text{CaO}$ , but also  $\text{CO}_2$  concentrations. Sample 444 comprises significant amorphous material (41 wt%) as well as notable clay (24.2 wt% of combined 14 Å clay and kaolinite), pyroxene, talc and hematite contents, imparting a significant  $\text{Fe}_2\text{O}_{3\text{tot}}$ ,  $\text{MgO}$ , moderate  $\text{SiO}_2$  and relatively low LOI concentrations. Sample 12779 contains 60 wt% combined K-feldspar and plagioclase and some 10 Å clay, translating into an  $\text{SiO}_2$ -,  $\text{Al}_2\text{O}_3$ - and  $\text{K}_2\text{O}$ -rich geochemical makeup. Finally, sample 3808 contains 98.5 wt% quartz and 1.5 wt% K-feldspar, giving a geochemical composition overwhelmed by  $\text{SiO}_2$  (estimated at 99.6 wt%); it probably also contains trace amounts of anatase or other Ti-bearing phase(s), undetected by the XRD method applied, to account for (some of) the 0.13 wt%  $\text{TiO}_2$  reported geochemically.

### 5.3 SPATIAL DISTRIBUTIONS OF THE $\text{SiO}_2$ IN NASGL A AND C HORIZONS

Maps of the distributions of estimated  $\text{SiO}_2$  concentrations in the NASGL A and C horizons are shown in Figures 5a and 5b, respectively. The data are classified in ten quantile (decile) classes and colored as per the mapping convention of Smith et al. (2014, 2019). The distributions show strong similarities with the backdrop quartz distribution maps in the A and C horizons (figures 140 and 141 in Smith et al. 2014, respectively), reflecting a dominant mineralogical control on the  $\text{SiO}_2$  concentrations.



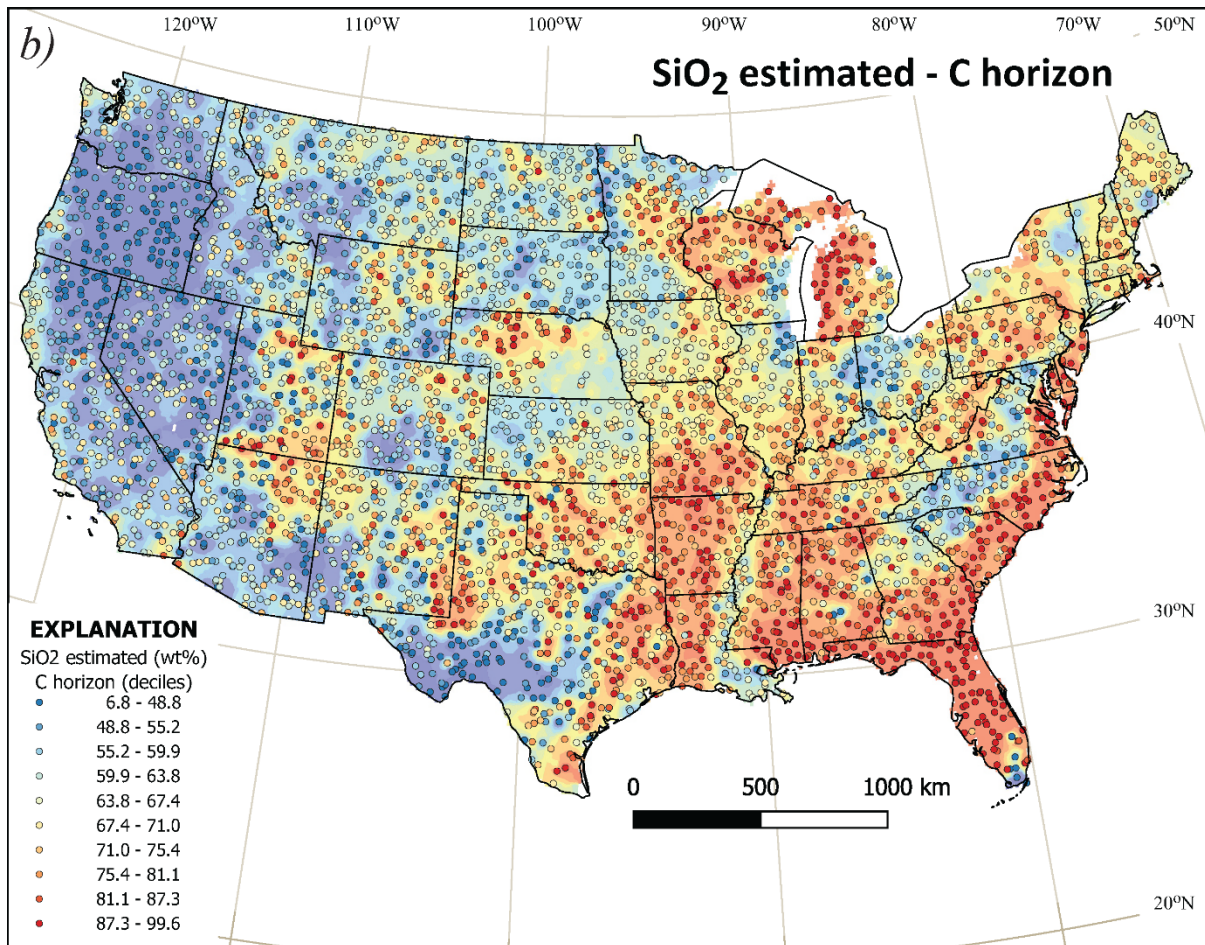


Figure 5. Spatial distributions of the SiO<sub>2</sub> concentrations estimated herein for the A horizon (a) and C horizon (b) of the NASGL samples. The symbols are classified and colored as per Smith et al. (2014), and overlain on the relevant quartz distribution interpolated maps (figures 140 and 141 in Smith et al. 2014, respectively).

## 5.4 VALIDATION

### 5.4.1 Application of Inversion Approach to Other Dataset

The proposed method to estimate the missing SiO<sub>2</sub> and LOI data was validated by applying it to an Exploring for the Future (EFTF; <http://www.ga.gov.au/eftf>) dataset (as yet unpublished) from Australia, which comprises geochemistry by XRF (including SiO<sub>2</sub>) and ICP-MS, and mineralogy by XRD. The dataset of 260 samples from the National Geochemical Survey of Australia (NGSA; Caritat & Cooper 2011a, Caritat 2022) crosses the continent from the temperate coast of South Australia (SA), through semi-arid parts of the Northern Territory (NT) and Queensland (Qld), to the tropical Gulf of Carpentaria coast, defining the SA-Qld-NT study area (large crosses in Figure 6). Thus a wide range of geological, geomorphological and climate conditions are intersected by this dataset, making it a suitable comparison to the NASGL dataset.

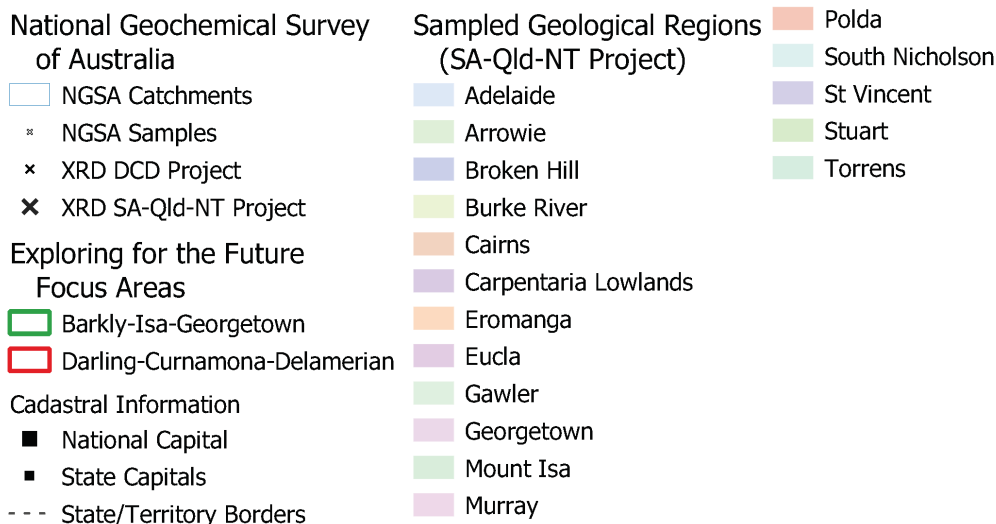
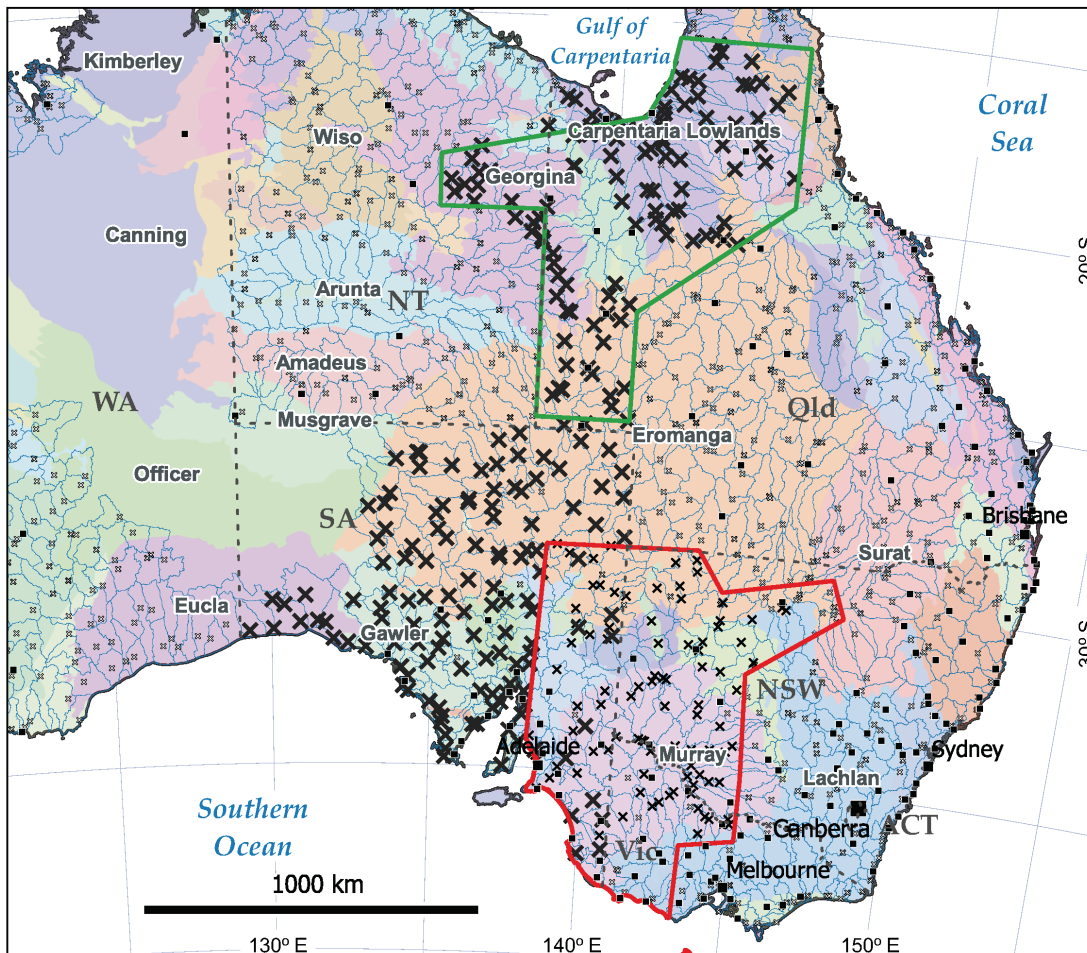


Figure 6. Distribution of selected NGS sample sites (large black crosses) analysed by XRF, ICP-MS and XRD in the SA-Qld-NT study area, overlain on Australia's geological regions (various colors; some with labels; Blake & Kilgour 1998). Acronyms used: NGS = National Geochemical Survey of Australia; DCD = Darling-Curnamona-Delamerian; SA = South Australia; Qld = Queensland; NT = Northern Territory. Modified after Caritat et al. (in press).

Figure 7 show the correlation between measured SiO<sub>2</sub> and estimated SiO<sub>2</sub> as per the recursive inversion method described herein for the SA-Qld-NT dataset. The correlation is linear, strong (R<sup>2</sup> = 0.91), with a slope close to unit (0.96), and a small intercept (1.7 wt%). The distribution is also fairly

homoscedastic. We interpret this to mean that the method to estimate SiO<sub>2</sub> in NASGL should be robust and widely applicable.

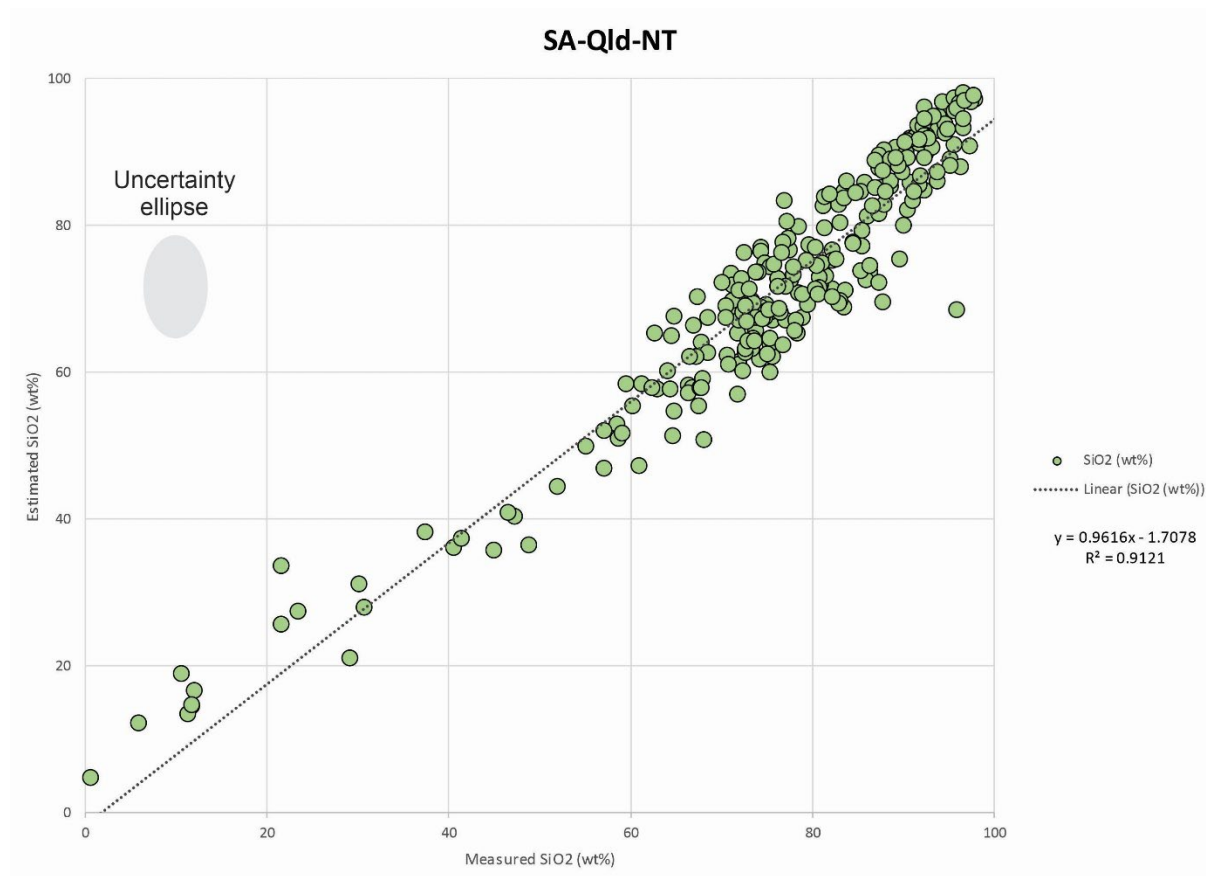


Figure 7. Scatterplot showing the relationship between SiO<sub>2</sub> concentrations estimated by the method described herein and measured by XRF in the SA-Qld-NT study area. The least squares linear regression is shown as a dotted line. Uncertainties (3 x SD) of 14 wt% and 7 wt% for estimated and measured SiO<sub>2</sub>, respectively (see Section 5.5), are illustrated by an ellipse.

#### 5.4.2 Comparison with Measured SiO<sub>2</sub>

A second validation approach was tested whereby the distributions obtained for the estimated SiO<sub>2</sub> in the C horizon of the NASGL samples were compared with measured SiO<sub>2</sub> in an independent dataset. The most extensive available dataset with SiO<sub>2</sub> concentrations in the USA to our knowledge is that of Shacklette & Boerngen (1984), albeit at a much lower spatial density than the NASGL project. They reported inorganic chemical analyses of soil and other regolith collected across the conterminous USA mostly during the 1960s and 1970s (no mineralogy is reported). The target medium was the subsoil at ~20 cm below surface to avoid any surface contamination; this depth commonly is within the range of a soil's B horizon, a zone of element accumulation (Boerngen & Shacklette 1981). Although more than 1300 sites were sampled in total, only 407 were analyzed for Si (by emission spectrography of the <2 mm grain size fraction) in 'Phase two' (~1969-1975) of the project (Shacklette & Boerngen 1984). The Si (wt%) concentrations were converted to SiO<sub>2</sub> (wt%) before use here.

Firstly the empirical distribution functions of the 'Shacklette & Boerngen' and NASGL datasets were compared using a Kolmogorov-Smirnov (K-S) test of distribution similarity (Kolmogorov 1933) (Figure

8). This non-parametric test quantifies the distance  $D$  separating an empirical distribution function from the cumulative distribution function of a reference distribution and an  $n$ -scaled critical value (CV). The null hypothesis ( $H_0$ ) being tested is that the two populations are indistinguishable and is quantified at a given probability  $p$ . The K-S test applied to the ‘Shacklette & Boerngen’ measured  $\text{SiO}_2$  concentrations and NASGL C horizon estimated  $\text{SiO}_2$  concentrations yields  $D = 0.0557$ , which is smaller than  $CV = 0.0703$ , therefore justifying accepting the  $H_0$  at  $p < 0.05$  (AAT Bioquest 2023).

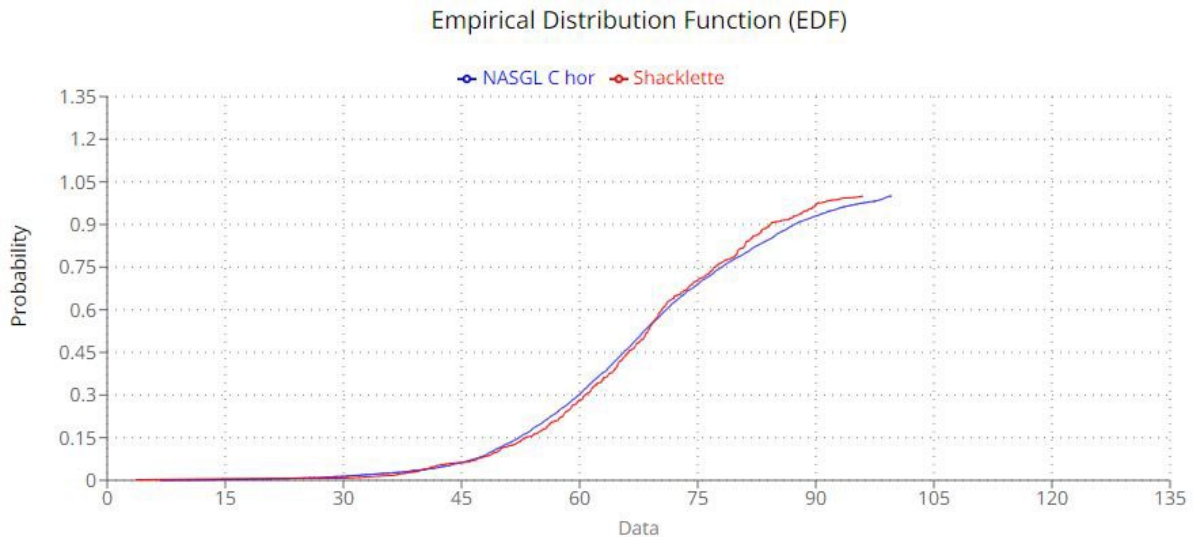


Figure 8. Empirical distribution functions of  $\text{SiO}_2$  concentrations estimated by the method described herein for NASGL C horizon samples ( $n = 4669$ ; blue line) and  $\text{SiO}_2$  measured by emission spectrography on the ‘Shacklette & Boerngen’ B horizon samples (‘Shacklette’; Shacklette & Boerngen 1984;  $n = 407$ ; red line).

Secondly a more rigorous test than comparing the general distributions, namely checking spatial consistency of  $\text{SiO}_2$  values, was applied. It has to be cautioned that (1) we are comparing two different soil horizons, B horizon in the ‘Shacklette & Boerngen’ dataset vs C horizon in the NASGL dataset; and (2) soil heterogeneity is present at all scales (e.g., Pedersen et al. 2015), implying that comparing sample pairs distant by even a few meters can give substantially different concentration values. Nonetheless we extracted the closest NASGL site to each ‘Shacklette & Boerngen’ site and filtered out those pairs where the distance between the two was 0.04 degrees of latitude/longitude ( $\sim 4$  km) or greater. The scatterplot and linear regression for the resulting subset are shown in Figure 9. The regression is surprisingly strong ( $R^2 = 0.79$ ) and with a slope close to unity (0.96). The relative standard deviation (RSD) on these pairs of sample (5%) is only marginally greater than the RSD on field duplicates obtained in the NGSA for  $\text{SiO}_2$  (4%; table 1 of Caritat & Cooper, 2011b), which is remarkable given the spatial distance between these ‘Shacklette & Boerngen’ and NASGL sites ( $\sim 1$  to 4 km) and their different sample media (B vs C horizons).

Overall, the above validation assessments give us confidence that the  $\text{SiO}_2$  estimates for the NASGL dataset, and by inference the recursive inversion methodology in general, stand up reasonably well when compared to ground-based measurements and experience from elsewhere.

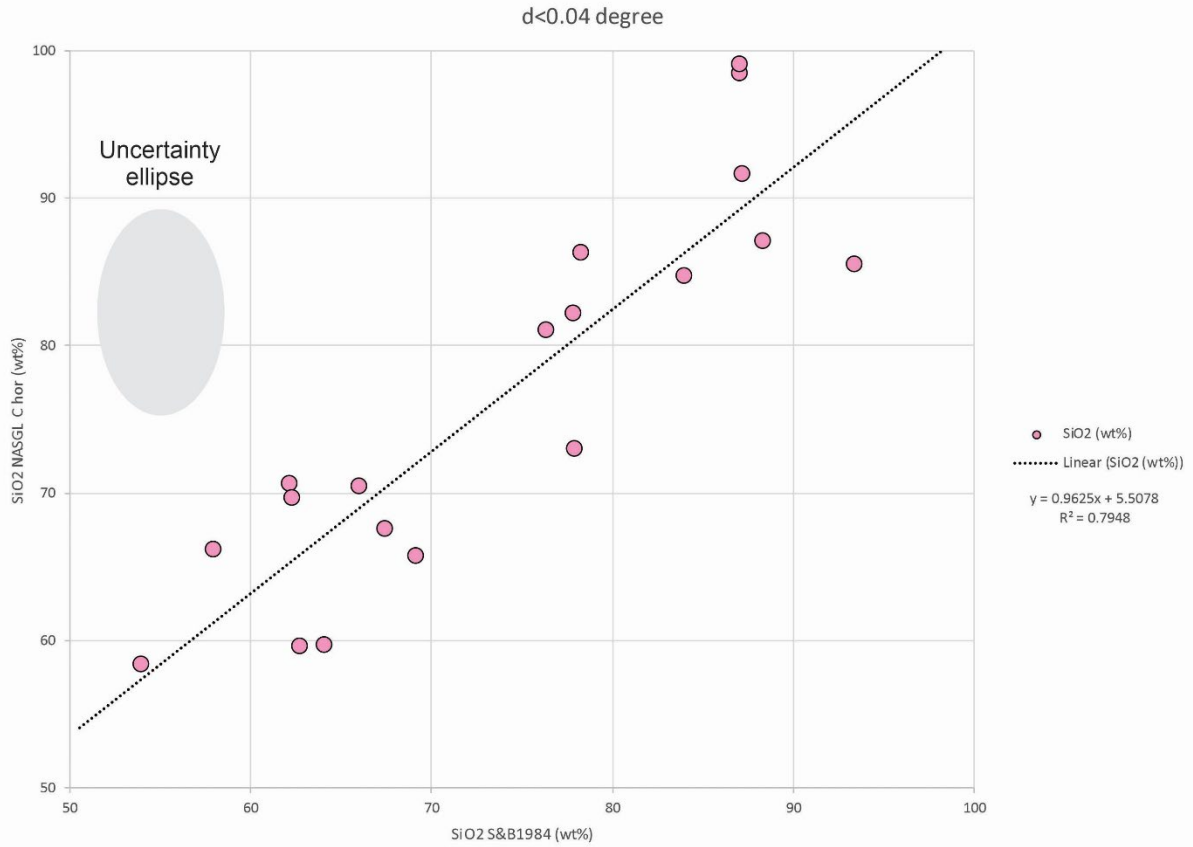


Figure 9. Scatterplot showing the relationship between  $\text{SiO}_2$  concentrations estimated by the method described herein for NASGL C horizon samples and  $\text{SiO}_2$  measured by emission spectrography on proximal (<~4 km) 'Shacklette & Boerngen' B horizon samples ('S&B1984'; Shacklette & Boerngen 1984;  $n = 19$ ). Uncertainties ( $3 \times \text{SD}$ ) of 14 wt% and 7 wt% for estimated and measured  $\text{SiO}_2$ , respectively (see Section 5.5), are illustrated by an ellipse.

## 5.5 UNCERTAINTY PROPAGATION

The uncertainty of the  $\text{SiO}_2$  estimates was investigated by propagating the errors as reported in Smith et al. (2013). As the  $\text{SiO}_2$  estimate is computed from a summation of measurements or elements  $e_j$ , its uncertainty,  $u_{\text{SiO}_2}$ , was determined using the root-sum-squares (RSS) method following Ellison et al. (1997) and Taylor (2005):

$$u_{\text{SiO}_2} = \pm \sqrt{e_1^2 + e_2^2 + \dots + e_k^2} = \pm \sqrt{\sum_{j=1}^k e_j^2},$$

where  $e_1 \dots e_k$  are the errors on the  $k$  elements that make up the variable. If we assume the error  $e$  of any measurement to be equal to three standard deviations (SDs) of that measurement,  $e_j = 3 \times \text{SD}_j$ , we get for  $n$  minerals involved in a measurement:

$$u_{\text{SiO}_2} = 3 \times \text{SD}_{\text{SiO}_2} = \pm \sqrt{(3 \times \text{SD}_{\text{mineral}_1})^2 + \dots + (3 \times \text{SD}_{\text{mineral}_n})^2}.$$

The  $\text{SiO}_2$  estimates in the NASGL datasets rely on the quantification of 18 silicates (to determine 'normative'  $\text{SiO}_2$ ), 12 hydrated minerals (to determine 'normative'  $\text{H}_2\text{O}$ ), and three carbonates (to determine 'normative'  $\text{CO}_2$ ) (Table 3). Thus 33 minerals overall are included in the estimates.

Conservatively utilizing a SD of 0.82 wt% for mineral quantification, the largest SD of any mineral reported by Smith et al. (2013, table 10), we derive:

$$u_{SiO_2} = 3 \times SD_{SiO_2} = \pm\sqrt{33 \times (3 \times 0.82)^2},$$

which gives an uncertainty for the SiO<sub>2</sub> estimates of 14.1 wt%. In comparison, the uncertainty of the XRF-based SiO<sub>2</sub> quantification in the NGSA is estimated at 7.3 wt% (three times the RSD of 0.04 x 61.06 wt% quoted in table 1 of Caritat & Cooper, 2011b).

## 5.6 LIMITATIONS

The current method of estimating SiO<sub>2</sub> when missing from a dataset can be applied to other situations, e.g. where ICP analysis has been used and Si not determined. However, as it currently stands, the methodology relies on mineralogical data being available for the same samples. Another limitation is that total or near-total geochemical analytical methods have to be used to ensure internal consistency with the mineralogical data; as such weak or partial digestion/leach techniques for sample preparation do not lend themselves directly to being compared with bulk mineralogy. Despite these limitations, there are many cases where (near-)total geochemical analysis and mineralogy have been determined, for instance in industry and government datasets.

## 5.7 FUTURE WORK

In a complementary approach in progress, we are developing a machine learning approach using linear regression and random forest algorithms to estimate SiO<sub>2</sub> where it is missing, based on geochemical information, mineralogical information, and both geochemical and mineralogical information. This method will be tested on various datasets, including the NASGL and SA-Qld-NT datasets, to ensure its universal applicability and will be reported separately (Grunsky et al. in prep.)

# 6 DATASETS

---

The original geochemical and mineralogical data for soils of the conterminous United States (A and C horizon datasets) were downloaded from <https://mrdata.usgs.gov/ds-801/>. The ‘Shacklette and Boerngen’ dataset was downloaded from <https://mrdata.usgs.gov/ussoils/>. A worked example for the five selected samples of Figure 5 is available as a Microsoft Excel spreadsheet (NALG\_Ch\_oxides\_with\_estimated\_SiO2\_LOI\_worked example.xlsx) here: <https://zenodo.org/record/8191288>. The new datasets including sample identification, coordinates, converted major oxide concentrations, and the concentration estimates for SiO<sub>2</sub> and LOI in wt% for the A and C horizon datasets from the North American Soil Geochemical Landscapes (NASGL) project are available as comma separated value files (NALG\_Ah\_oxides\_with\_estimated\_SiO2\_LOI.csv and NALG\_Ch\_oxides\_with\_estimated\_SiO2\_LOI.csv) here: <https://zenodo.org/record/8191288>.

# 7 CONCLUSIONS

---

We provide a novel method for estimating the concentrations of silica (SiO<sub>2</sub> wt%) and loss-on-ignition (LOI wt%) in the North American Soil Geochemical Landscapes (NASGL) project datasets. These datasets include comprehensive elemental and mineralogical compositions, determined mostly by four-acid digestion Inductively Coupled Plasma (ICP) Atomic Emission Spectroscopy (AES) or Mass Spectrometry (MS), depending on the element, and Rietveld refinement X-Ray Diffraction

(XRD), respectively. Unfortunately, neither Si/SiO<sub>2</sub> nor LOI are quantified, both of which are significant components of most soils. Our estimation method combines the precision of the ICP determinations with the completeness of the XRD data. As the NASGL samples contain up to 95 wt% amorphous material of unknown geochemical or mineralogical composition, it is not possible to directly calculate SiO<sub>2</sub> or LOI contents from mineralogy alone. However, a recursive inversion approach, i.e., calculating geochemistry from mineralogy, can be invoked to calculate minimum SiO<sub>2</sub>, H<sub>2</sub>O and CO<sub>2</sub> concentrations. Thus, we inverted an estimate for SiO<sub>2</sub> by adding up the SiO<sub>2</sub> contributions from all Si-bearing minerals (silicates). This 'normative' SiO<sub>2</sub> represents a *minimum* estimation of the total SiO<sub>2</sub> in each sample. Similarly, we inverted estimates for H<sub>2</sub>O by adding up the H<sub>2</sub>O contributions from all O-H-bearing minerals (hydrates), and for CO<sub>2</sub> by adding up the CO<sub>2</sub> contributions from all C-bearing minerals (carbonates). Combining the latter two components gives a minimum estimate for LOI. Thus, **100 wt% - (all major oxides from ICP + TEs from ICP + 'normative' H<sub>2</sub>O + 'normative' CO<sub>2</sub>)**, yields a *maximum* estimate of the total SiO<sub>2</sub> in each sample. The final or 'consensus' SiO<sub>2</sub> estimate is then calculated as the average between the two aforementioned estimates, trimmed as necessary to yield a total composition **(all major oxides from ICP + estimated SiO<sub>2</sub> + TEs from ICP + 'normative' H<sub>2</sub>O + 'normative' CO<sub>2</sub>)** of no more than 100 wt%. For most samples, the above sum falls below 100 wt% and the difference is taken to represent LOI not otherwise accounted for in the quantified hydrate and carbonate minerals. The source of this LOI contribution likely includes H<sub>2</sub>O and CO<sub>2</sub> in the amorphous phase as well as other volatile components present in soil. We examine the statistical distributions of the SiO<sub>2</sub> and LOI estimates and validate the technique against a separate dataset from Australia where XRF, ICP and XRD data on the same samples exist. The correlation between predicted and observed SiO<sub>2</sub> is deemed strong (R<sup>2</sup> = 0.91). Further we compared the estimated NASGL C horizon SiO<sub>2</sub> estimates with an independent dataset covering the conterminous USA, the 'Shacklette and Boerngen' dataset. The distributions of these two datasets are shown by a Kolmogorov-Smirnov test to be statistically identical. Spatially we demonstrate that the closest NAGSL sites and 'Shacklette and Boerngen' sites have highly correlated SiO<sub>2</sub> concentrations (R<sup>2</sup> = 0.79). Together, these validation assessments give us the confidence to recommend the approach of combining geochemical and mineralogical datasets to estimate missing SiO<sub>2</sub> and LOI in datasets elsewhere. However, as each situation is different, any estimation results ideally should be ground-truthed.

## 8 ACKNOWLEDGMENTS

---

The estimation method and Australian validation study were conducted as part of Geoscience Australia's Exploring for the Future (EFTF; <https://www.eftf.ga.gov.au/>) program, which provides precompetitive information to inform decision-making by government, community and industry on the sustainable development of Australia's mineral, energy and groundwater resources. By gathering, analysing and interpreting new and existing precompetitive geoscience data and knowledge, the EFTF is building a national picture of Australia's geology and resource potential. This leads to a strong economy, resilient society and sustainable environment for the benefit of all Australians. This includes supporting Australia's transition to net zero emissions, strong, sustainable resources and agriculture sectors, and economic opportunities and social benefits for Australia's regional and remote communities. The EFTF program, which commenced in 2016, is an eight year, \$225m investment by the Australian Government. The authors appreciate comments on a draft version of this manuscript by Laurel G. Woodruff (United States Geological Survey) as well as internal

reviews by Philip Main, Tara Webster and Anthony Schofield (Geoscience Australia). PdC publishes with permission from the Chief Executive Officer, Geoscience Australia.

## 9 REFERENCES

---

AAT Bioquest, 2023. Quest Graph™ Kolmogorov-Smirnov (K-S) Test Calculator.

<https://www.aatbio.com/tools/kolmogorov-smirnov-k-s-test-calculator>

Achilles, C.N., Downs, G.W., Downs, R.T., Morris, R.V., Rampe, E.B., Ming, D.W., Chipera, S.J., Blake, D.F., Vaniman, D.T., Bristow, T.F., Yen, A.S., Morrison, S.M., Treiman, A.H., Craig, P.I., Hazen, R.M., Tu, V.M. & Castle, N., 2018. Amorphous phase characterization through X-ray diffraction profile modeling: implications for amorphous phases in Gale Crater rocks and soils. 49th Lunar and Planetary Science Conference, LPI Contribution 2083, 2661.

<https://www.hou.usra.edu/meetings/lpsc2018/pdf/2661.pdf>

Aitchison, J., 1986. The Statistical Analysis of Compositional Data. Chapman and Hall, London, 416 p. ISBN 9781930665781.

Aldis, M., Posch, M. & Aherne, J., 2023. Normative mineralogy of 1170 soil profiles across Canada. Minerals, 13, 544. <https://doi.org/10.3390/min13040544>

Blake D. & Kilgour B., 1998. Geological Regions of Australia 1:5 000 000 Scale. Geoscience Australia, Dataset. <http://pid.geoscience.gov.au/dataset/ga/32366>

Boerngen, J.G. & Shacklette, H.T., 1981. Chemical Analyses of Soils and Other Surficial Materials of the Conterminous United States. United States Geological Survey, Open-File Report, 81-197, 143 p. <https://doi.org/10.3133/ofr81197>

Box, G.E.P. and Cox, D.R., 1964. An analysis of transformations. Journal of the Royal Statistical Society, Series B, 26, 211–252. <https://doi.org/10.1111/j.2517-6161.1964.tb00553.x>

Caritat, P. de & Cooper, M., 2011a. National Geochemical Survey of Australia: The Geochemical Atlas of Australia. Geoscience Australia, Record, 2011/20, 557 p. <http://dx.doi.org/10.11636/Record.2011.020>

Caritat, P. de & Cooper, M., 2011b. National Geochemical Survey of Australia: Data Quality Assessment. Geoscience Australia, Record, 2011/021, 478 p. <https://pid.geoscience.gov.au/dataset/ga/71971>

Caritat, P. de, 2022. The National Geochemical Survey of Australia: review and impact. Geochemistry: Exploration, Environment, Analysis, 22, geochem2022-032. <https://doi.org/10.1144/geochem2022-032>

Caritat, P. de, Bloch, J. & Hutcheon, I., 1994. LPNORM: a linear programming normative analysis code. Computers & Geosciences, 20, 313–347. [https://doi.org/10.1016/0098-3004\(94\)90045-0](https://doi.org/10.1016/0098-3004(94)90045-0)

Caritat, P. de, Petts, A. & Kelaart, C., in press. Contribution Towards a Regolith Mineralogy Map of the Australian Continent: A Study in South Australia, Queensland and the Northern Territory. Geoscience Australia, Record, 2023.

Chayes, F., 1960. On correlation between variables of constant sum. Journal of Geophysical Research, 65, 4185–4193. <https://doi.org/10.1029/JZ065i012p04185>

- Deer, W.A., Howie, R.A. & Zussman, J., 2013. An Introduction to the Rock-Forming Minerals, 3rd edition. Mineralogical Society of Great Britain and Ireland, 498 p. ISBN 9780903056274.
- Ellison, S., Wegscheider, W. & Williams, A., 1997. Measurement uncertainty. *Analytical Chemistry*, 69, 607A–613A. <https://doi.org/10.1021/ac971793j>
- Finkl, C.W., 1981. Soil mineralogy. In: *Mineralogy, Encyclopedia of Earth Science*. Springer, Boston, MA. [https://doi.org/10.1007/0-387-30720-6\\_133](https://doi.org/10.1007/0-387-30720-6_133)
- Grunsky, E.C., Drew, L.J. & Smith, D.B., 2018. Analysis of the United States portion of the North American Soil Geochemical Landscapes Project – A compositional framework approach. In: Daya Sagar, B., Cheng, Q. & Agterberg, F. (eds), *Handbook on Mathematical Geosciences*, Springer, Cham, 313–346. ISBN 9783319789996. [https://doi.org/10.1007/978-3-319-78999-6\\_17](https://doi.org/10.1007/978-3-319-78999-6_17)
- Kolmogorov, A.N., 1933. Sulla determinazione empirica di una legge di distribuzione. *Giornale dell'Istituto Italiano degli Attuari*, 4, 83–91. [No DOI]
- Mann, A.W., 2010. Strong versus weak digestions: ligand-based soil extraction geochemistry. *Geochemistry: Exploration, Environment, Analysis*, 10, 17–26. <https://doi.org/10.1144/1467-7873/09-216>
- Palarea-Albaladejo, J., Martín-Fernández, J.A. & Buccianti, A., 2014. Compositional methods for estimating elemental concentrations below the limit of detection in practice using R. *Journal of Geochemical Exploration*, 141, 71–77. <https://doi.org/10.1016/j.gexplo.2013.09.003>
- Pedersen, L.L., Smets, B.F. & Dechesne, A., 2015. Measuring biogeochemical heterogeneity at the micro scale in soils and sediments. *Soil Biology and Biochemistry*, 90, 122–138. <https://doi.org/10.1016/j.soilbio.2015.08.003>
- Scealy, J.L., Caritat, P. de, Grunsky, E.C., Tsagris, M.T. & Welsh, A.H., 2015. Robust principal component analysis for power transformed compositional data. *Journal of the American Statistical Association*, 110, 136–148. <https://doi.org/10.1080/01621459.2014.990563>
- Schaetzl, R. & Anderson, S., 2007. *Soils – Genesis and Geomorphology*, 1<sup>st</sup> edition reprinted with corrections. Cambridge University Press, Cambridge, 817 p. ISBN 9780521812016.
- Shacklette, H.T. & Boerngen, J.G., 1984. *Element Concentrations in Soils and Other Surficial Materials of the Conterminous United States: An Account of the Concentrations of 50 Chemical Elements in Samples of Soils and Other Regoliths*. United States Geological Survey, Professional Paper, 1270, 105 p. <https://pubs.usgs.gov/pp/1270/>
- Smith, D.B., 2022. Geochemical and mineralogical soil survey of the conterminous USA: a project retrospective. *Geochemistry: Exploration, Environment, Analysis*, 22, geochem2022-031. <https://doi.org/10.1144/geochem2022-031>
- Smith, D.B., Cannon, W.F., Woodruff, L.G. & Ellefsen, K.J., 2014. *Geochemical and Mineralogical Maps for Soils of the Conterminous United States*. United States Geological Survey, Open-File Report, 2014-1082, 386 p. <https://doi.org/10.3133/ofr20141082>
- Smith, D.B., Cannon, W.F., Woodruff, L.G., Solano, Federico, Kilburn, J.E. & Fey, D.L., 2013. *Geochemical and Mineralogical Data for Soils of the Conterminous United States*. United States Geological Survey, Data Series, 801, 19 p. <http://pubs.usgs.gov/ds/801>

Smith, D.B., Solano, F., Woodruff, L.G., Cannon, W.F. & Ellefsen, K.J., 2019. Geochemical and Mineralogical Maps, with Interpretation, for Soils of the Conterminous United States. United States Geological Survey, Scientific Investigations Report, 2017-5118.

<https://pubs.usgs.gov/sir/2017/5118/index.html>

Smith, R.J., Horgan, B., Rampe, E. & Dehouck, E., 2018. The composition of amorphous phases in soils and sediments on earth and Mars. 49th Lunar and Planetary Science Conference, LPI Contribution 2083, 1779. <https://www.hou.usra.edu/meetings/lpsc2018/pdf/1779.pdf>

Tan, K.H., Perkins, H.F. & McCreery, R.A., 1970. The nature and composition of amorphous material and free oxides in some temperate region and tropical soils. Communications in Soil Science and Plant Analysis, 1, 227–238. <https://doi.org/10.1080/00103627009366262>

Taylor, J.A., 2005. Uncertainty Analysis. ES 223: Rigid Body Dynamics-Fall 2004. Arkansas State University, Jonesboro, AR. Online Lecture Notes.

<http://myweb.astate.edu/sharan/PMC/LectureNotes/2006/Paper%20on%20Uncertainty%20Analysis.pdf>

Tsukimura, K., Miyoshi, Y., Takagi, T., Suzuki, M. & Wada, S., 2021. Amorphous nanoparticles in clays, soils and marine sediments analyzed with a small angle X-ray scattering (SAXS) method. Scientific Reports, 11, 6997. <https://doi.org/10.1038/s41598-021-86573-9>

Tukey, J.W., 1977. Exploratory Data Analysis. Addison-Wesley Publishing Company, Reading, MA, 688 p. ISBN 9780201076165.